

# Transposable element profiles reveal cell line identity and loss of heterozygosity in *Drosophila* cell culture

Shunhua Han <sup>1</sup>, Preston J. Basting,<sup>1</sup> Guilherme B. Dias ,<sup>1,2</sup> Arthur Luhur ,<sup>3,4</sup> Andrew C. Zelfhof ,<sup>3,4</sup> and Casey M. Bergman <sup>1,2,\*</sup>

<sup>1</sup>Department of Genetics and Institute of Bioinformatics, University of Georgia, Athens, GA 30602, USA,

<sup>2</sup>Department of Genetics, University of Georgia, Athens, GA 30602, USA,

<sup>3</sup>Drosophila Genomics Resource Center, Indiana University, Bloomington, IN 47405, USA, and

<sup>4</sup>Department of Biology, Indiana University, Bloomington, IN 47405, USA

\*Corresponding author: University of Georgia, Athens, GA 30602, USA. Email: cbergman@uga.edu

## Abstract

Cell culture systems allow key insights into biological mechanisms yet suffer from irreproducible outcomes in part because of cross-contamination or mislabeling of cell lines. Cell line misidentification can be mitigated by the use of genotyping protocols, which have been developed for human cell lines but are lacking for many important model species. Here, we leverage the classical observation that transposable elements (TEs) proliferate in cultured *Drosophila* cells to demonstrate that genome-wide TE insertion profiles can reveal the identity and provenance of *Drosophila* cell lines. We identify multiple cases where TE profiles clarify the origin of *Drosophila* cell lines (Sg4, mbn2, and OSS\_E) relative to published reports, and also provide evidence that insertions from only a subset of long-terminal repeat retrotransposon families are necessary to mark *Drosophila* cell line identity. We also develop a new bioinformatics approach to detect TE insertions and estimate intra-sample allele frequencies in legacy whole-genome sequencing data (called ngs\_te\_mapper2), which revealed loss of heterozygosity as a mechanism shaping the unique TE profiles that identify *Drosophila* cell lines. Our work contributes to the general understanding of the forces impacting metazoan genomes as they evolve in cell culture and paves the way for high-throughput protocols that use TE insertions to authenticate cell lines in *Drosophila* and other organisms.

**Keywords:** *Drosophila*; transposable element; cell culture; cell line authentication; loss of heterozygosity

## Introduction

Cultured cell lines play essential roles in biological research, providing model systems to support discovery of basic molecular mechanisms and tools to produce biomolecules with medical and industrial relevance. Despite their widespread use, experiments in cultured cells often show non-reproducible outcomes, and increasing the rigor of cell line-based research is a priority of both funders and journals alike (Lorsch et al. 2014). One major source of irreproducible research comes from mislabeling or cross-contamination of cell lines (collectively referred to here as “misidentification”), resulting in cells of the wrong type or species being used in a particular study (Defendi et al. 1960; Gartler 1967; Nelson-Rees et al. 1981; MacLeod et al. 1999; Huang et al. 2017). As such, substantial effort has been invested into minimizing cell line misidentification through genotyping cell lines, cataloging misidentified lines, standardizing cell line nomenclature, and the use of research resource identifiers (Masters et al. 2001; Barallon et al. 2010; Capes-Davis et al. 2010; Yu et al. 2015; Babic et al. 2019).

Starting with the first reports on the cell line misidentification problem, a variety of cytological and molecular techniques have been developed to authenticate mammalian cell lines (Defendi et al. 1960;

Gartler 1967; O'Brien et al. 1977; Gilbert et al. 1990; Masters et al. 2001; Castro et al. 2013). These efforts culminated in the development of short tandem repeats (STRs) as a widely used standard to authenticate human cell lines at the molecular level (Masters et al. 2001; Barallon et al. 2010; Almeida et al. 2016). STR-based authentication has mitigated—but not eradicated—the human cell line misidentification problem, in part because of limitations in the stability, measurement, and matching of STRs (Parson et al. 2005; American Type Culture Collection Standards Development Organization Workgroup ASN-0002 2010; Yu et al. 2015; Horbach and Halffman 2017). More recently, alternative methods for genotyping human cell lines based on single nucleotide polymorphisms (SNPs) have been developed (Castro et al. 2013; Liang-Chu et al. 2015; Yu et al. 2015; Zaaier et al. 2017; Mohammad et al. 2019), but these methods have not yet been accepted as standards for cell line authentication in humans (Almeida et al. 2016).

For most species beside humans, cell line authentication standards and protocols remain to be established (Almeida et al. 2016). For example, no protocols currently exist to authenticate cell lines in the fruit fly *Drosophila melanogaster*, despite the existence of over 150 different cell lines for this model animal system (Luhur et al. 2019). As such, no evidence of misidentified *Drosophila* cell lines has been

Received: May 01, 2021. Accepted: July 01, 2021

© The Author(s) 2021. Published by Oxford University Press on behalf of Genetics Society of America.

This is an Open Access article distributed under the terms of the Creative Commons Attribution License (<http://creativecommons.org/licenses/by/4.0/>), which permits unrestricted reuse, distribution, and reproduction in any medium, provided the original work is properly cited.

cataloged to date by the International Cell Line Authentication Committee (v10, <https://iclac.org/databases/cross-contaminations/>). The development of cell line identification protocols and standards for common model organisms like *Drosophila* is an important goal for increasing rigor and reproducibility in bioscience. Achieving this goal for a new species requires an understanding of the genome biology and cell line diversity of that organism, and should ideally take advantage of powerful, cost-effective modern genomic technologies.

Relative to humans, the STR mutation rate is low in *D. melanogaster* (Schug et al. 1997) and thus the use of STRs for discriminating different *Drosophila* cell lines is likely to be limited. In contrast, it is well-established that transposable element (TE) insertions are highly polymorphic among individual flies (Charlesworth and Langley 1989) that TE abundance is elevated in *Drosophila* cell lines relative to whole flies (Potter et al. 1979; Ilyin et al. 1980; Rahman et al. 2015), and that TE families amplified in cell culture vary among *Drosophila* cell lines (Echalier 1997; Rahman et al. 2015). These properties suggest that TE insertions should be useful markers to discriminate different cell lines established from distinct *D. melanogaster* donor genotypes (e.g., S2 vs Kc cells) and possibly also from the same donor genotype, including divergent sublines of the same cell line (e.g., S2 vs S2R+ cells) (Echalier and Ohanessian 1969; Schneider 1972; Yanagawa et al. 1998). Indeed, previous studies have shown that *D. melanogaster* cell lines have unique TE landscapes and that sublines of the same cell line often share a higher proportion of TE insertions relative to distinct cell lines (Sytņnikova et al. 2014; Rahman et al. 2015).

Here, we show that *Drosophila* cell lines can successfully be clustered and identified on the basis of their genome-wide TE profiles using a combination of publicly available paired-end short-read whole-genome sequencing (WGS) data from the modENCODE project (Lee et al. 2014) and new WGS data for eight widely used *Drosophila* cell lines. Our approach reveals the first examples where the reported provenance of *Drosophila* cell lines—Sg4 (Morales et al. 2004) and mbn2 (Gateff et al. 1980)—conflicts with identity inferred from genomic data. Importantly, our TE-based clustering approach also allows us to identify which subset of TE families discriminate the most widely used *Drosophila* cell lines, paving the way for the development of PCR-based genotyping protocols that can be used for cost-effective *Drosophila* cell line identification.

Additionally, we develop a new tool for the detection of TEs in single-end WGS data (called “ngs\_te\_mapper2”) and integrate our new data with legacy data (Sienski et al. 2012; Sytņnikova et al. 2014) to resolve the history and provenance of the widely used OSS and OSC ovarian cell lines (Niki et al. 2006; Saito et al. 2009). Using TE-based clustering, we provide evidence that OSS and OSC cell lines can be discriminated on the basis of the ZAM retrotransposon family. We propose that the OSS\_E subline reported in Sytņnikova et al. (2014) approximates an ancestral state of the OSC cell line, with contemporary OSC sublines having undergone loss of heterozygosity (LOH) in cell culture from an OSS\_E-like state. Together, our results show that TE insertions are a powerful source of genetic markers that can be used for cell line authentication in *Drosophila* and that LOH is an important mechanism driving *Drosophila* cell line genome evolution.

## Materials and methods

### Genome sequencing

Public genome sequencing data for 26 samples of 18 *Drosophila* cell lines were obtained from the modENCODE project (Lee et al. 2014). Frozen stocks of eight additional samples from six

*Drosophila* cell lines (mbn2, Sg4, ML-DmBG3-c2, ML-DmBG2-c2, OSS, and OSC) were obtained from the *Drosophila* Genomics Resource Center (DGRC), the Gorski lab (Canada’s Michael Smith Genome Sciences Centre, BC Cancer) and the Strand lab (University of Georgia). DNA extractions were performed using Qiagen Blood and Tissue kit (Cat# 69504) for the mbn2 sample from the Strand lab and using the Zymo-Quick kit (Cat# D4068) for all other samples. Purified DNA was analyzed by Qubit and Fragment Analyzer to determine the concentration and size distribution, respectively. Samples were normalized to the same concentration before preparing libraries with the KAPA Hyper Prep Kit (Cat# KK8504). During library prep, DNA was fragmented by acoustic shearing with Covaris E220 Evolution before end repair and A-tailing. Single indices were ligated to DNA fragments. Libraries were purified and cleaned with Solid Phase Reversible Immobilization (SPRI) beads before PCR amplification. Final libraries underwent an additional round of bead cleanup before being assessed by Qubit, qPCR (KAPA Library Quantification Kit Cat# KK4854), and Fragment Analyzer. Libraries were then sequenced in paired-end 150-bp mode on an Illumina NextSeq500 high output flowcell and demultiplexed using bcl2fastq. Metadata, sequencing statistics, and SRA accession numbers for all cell line DNA-seq samples used in this study can be found in [Supplementary Table S1](#).

### Detection of non-reference TE insertions using paired-end sequencing data

Paired-end sequencing data from the modENCODE project (Lee et al. 2014) and our study were used as input to seven methods designed to detect non-reference TE insertions in *Drosophila* (Kofler et al. 2012, 2016; Linheiro and Bergman 2012; Zhuang et al. 2014; Adrion et al. 2017; Yu et al. 2021) using McClintock (revision 40863acf11052b18afb4cdcd7b1124de48cba397; options: -m “trimgalore, popoolationte, popoolationte2, temp, temp2, teflon, ngs\_te\_mapper, ngs\_te\_mapper2”) (Nelson et al. 2017). Additionally, we predicted non-reference TE insertions using a version of TIDAL 1.2 (Rahman et al. 2015; Yang et al. 2021) that was modified to output results in a format compatible with results from McClintock (<https://github.com/bergmanlab/TIDAL>, revision 2d110b17b3b287dbc1ceb67c87fe171d15095c84). The reference genome for these analyses was comprised of the major chromosome arms from the *D. melanogaster* dm6 assembly (chr2L, chr2R, chr3L, chr3R, chr4, chrM, chrY, and chrX) and the TE library was the Berkeley *Drosophila* Genome Project canonical TE dataset v10.1 ([https://github.com/bergmanlab/transposons/blob/master/releases/D\\_mel\\_transposon\\_sequence\\_set\\_v10.1.fa](https://github.com/bergmanlab/transposons/blob/master/releases/D_mel_transposon_sequence_set_v10.1.fa); revision f94d53ea10b95c9da99258ac2336ce18871768e9).

Paired-end samples analyzed here vary substantially in read length (50–151 bp) and depth of coverage (5X–136X; [Supplementary Table S1](#)). We chose not to normalize input datasets by downsampling to the lowest read length and coverage to avoid reducing the sensitivity of non-reference TE detection methods for higher-quality samples. Using complete samples allowed us to observe that the number of non-reference TE predictions per sample ([Supplementary Table S2](#)) showed a strong dependence on read length ([Supplementary Figure S1](#)) or coverage ([Supplementary Figure S2](#)) for all methods besides TEMP (Zhuang et al. 2014). Thus, we used TEMP predictions with default McClintock filtering (retain only 1p1 predictions with >0.1 intra-sample allele frequency cutoff) for the global analysis of the modENCODE-only and expanded (modENCODE plus new samples) datasets. To resolve details of the relationship among mbn2 sublines, we used read length and coverage normalized mbn2

samples with relaxed filtering criteria for TEMP predictions (retain all 1p1/2p/singleton predictions with no intra-sample allele frequency cutoff).

### Detection of non-reference TE insertions using single-end sequencing data

Single-end sequencing data for OSS and OSC cell line samples from two previous studies (Sienski et al. 2012; Sytnikova et al. 2014) and forward reads from our paired-end samples were used to predict non-reference TE insertions using `ngs_te_mapper2` ([https://github.com/bergmanlab/ngs\\_te\\_mapper2](https://github.com/bergmanlab/ngs_te_mapper2)) in McClintock (revision 40863acf11052b18afb4cdcd7b1124de48cba397; options: `-m "trimgalore, coverage, ngs_te_mapper2, map_reads"`; Nelson et al. 2017). `ngs_te_mapper2` is a reimplement of the non-reference TE detection method initially reported in Linheiro and Bergman (2012) that improves speed and sensitivity and has been extended to estimate TE allele frequency (see Supplementary Text for details). Reference genome and TE library files used for McClintock runs on single-end sequencing data were the same as used above for paired-end sequencing data. Because `ngs_te_mapper2` detection rates and allele frequency estimates are sensitive to read length and depth of coverage (see Supplementary Text), reads from single-end sequencing data and the forward read of our paired-end sequencing data were normalized by trimming all reads to 100 bp using `fastp v0.20.1` (Chen et al. 2018) and downsampling to the lowest coverage sample (14X) using `seqtk v1.3` (Li 2015).

### Classification of intra-sample TE insertion allele frequency

To predict whether TE insertions within OSS and OSC cell line samples were heterozygous or homozygous, we built a classifier that uses allele frequencies estimated by `ngs_te_mapper2` from single-end sequencing data as input. A non-reference TE insertion was predicted to be heterozygous if the intra-sample allele frequency estimated by `ngs_te_mapper2` is between 0.25 and 0.75 and predicted to be homozygous if the intra-sample allele frequency is greater than or equal to 0.95. TE insertions with intra-sample allele frequencies outside these ranges were considered unclassified. The classifier was benchmarked using synthetic homozygous and heterozygous WGS datasets created with `wgsim v0.3.1-r13` using the ISO1 (dm6) and A4 (GCA\_003401745.1; Chakraborty et al. 2018) genome assemblies as input. The classifier yields >91% precision using input from the results of `ngs_te_mapper2` applied to the simulated datasets (see Supplementary Text for details).

### Identification of orthologous TE insertions

Because positional resolution of non-reference TE predictions is inexact (Nelson et al. 2017), we identified a high-quality set of orthologous non-reference TE insertion loci as follows. Genome-wide non-redundant BED files of non-reference TE predictions generated by McClintock were filtered to exclude TEs in low recombination regions using boundaries defined by Cridland et al. (2013) lifted over to dm6 coordinates. Normal recombination regions included in our analyses were defined as chrX: 405,967–20,928,973, chr2L: 200,000–20,100,000, chr2R: 6,412,495–25,112,477, chr3L: 100,000–21,906,900, chr3R: 4,774,278–31,974,278. We restricted our analysis to normal recombination regions, since low recombination regions have high reference TE content which reduces the ability to predict non-reference TE insertions (Bergman et al. 2006; Manee et al. 2018). We also excluded INE-1 family from our analysis, as this family is reported to be inactive for millions of years (Singh and Petrov 2004; Wang et al. 2007).

Non-reference TE predictions in high recombination from all samples were then clustered into orthologous loci using `BEDtools cluster v2.26.0` enforcing predictions within each cluster to be on the same strand (option `-s`; Quinlan and Hall 2010). Orthologous loci were then filtered using the following criteria: (1) retain only a single TE family per locus; (2) retain only a single TE prediction per sample per locus; and (3) retain TE predictions only from long-terminal repeat (LTR) retrotransposon, LINE-like retrotransposon or DNA transposon families. For clustering of paired-end samples, we imposed the additional filtering requirement that all clusters include at least sample per locus with a TEMP 1p1 prediction.

### Clustering and identification of cell line samples using TE insertion profiles

Non-reference TE predictions at orthologous loci were then converted to a binary presence/absence matrix in order to cluster cell lines on the basis of their TE insertion profiles. Cell line clustering was performed using Dollo parsimony in `PAUP (v4.0a168; Swofford 2003)`. Dollo parsimony analyses were conducted using heuristic searches with 50 replicates. A hypothetical ancestor carrying the assumed ancestral state for each locus (absence) was included as a root in the analysis (Batzer and Deininger 2002). “DescribeTrees chgList = yes” option was used to assign character state changes to branches in the tree. Node support for the most parsimonious tree was evaluated by integrating 100 bootstrap replicates generated by `PAUP` using `SumTrees (Sukumaran and Holder 2010)`.

Identification of a cell line sample was performed by adding its TE profile to a binary presence/absence matrix of “primary replicates” of 22 non-redundant *Drosophila* cell line samples and performing cell line clustering using the same approach mentioned above. A phylogenetic tree of the 22 non-redundant primary *Drosophila* cell line samples was used as a backbone topological constraint during a heuristic searches for the most parsimonious tree that included one additional “secondary replicate.” Node support for the most parsimonious tree was evaluated by integrating 100 bootstrap replicates without topological constraints.

### B-allele frequency and copy number analysis

BAM files generated by McClintock were used for variant calling using `bcftools v1.9` (Li 2011). Indels were excluded from variant calling, leaving only SNPs in the VCF file. For a given SNP, the B-allele frequency (BAF) was determined as the coverage of reads supporting non-reference allele divided by total coverage at that position using the `DP4` field.

BAM files generated by McClintock were also used to generate copy number variant (CNV) profiles for nonoverlapping 10-kb windows of the dm6 genome using `Control-FREEC (v11.6; Boeva et al. 2012)`. Windows with less than 85% mappability were excluded from the analysis based on mappability tracks generated by `GEM (v1.315 beta; Derrien et al. 2012)`. The baseline ploidy was determined by normalized DNA read density of 10-kb windows following Lee et al. (2014). The sex information was determined from relative read density between chromosome X and autosomes. The minimum and maximum expected value of the GC content was set to be 0.3 and 0.45, respectively.

### Clustering of cell line samples based on transcriptomes

Total RNA-sequencing samples for 17 *Drosophila* cell lines with 100-bp paired-end reads were obtained from Stoiber et al. (2016)

and from the modENCODE *D. melanogaster* transcriptome sequencing project (Brown et al. 2014). SRA accession numbers for all cell line RNA-seq samples used in this analysis can be found in Supplementary Table S3. Transcript abundances for protein-coding genes were quantified in unit of transcripts per million using kallisto quant v0.46.2 (Bray et al. 2016) using the release 6.32 version of the *D. melanogaster* transcript coding sequences corresponding to Ensembl genes from Ensembl release 103 ([http://ftp.ensembl.org/pub/release-103/fasta/drosophila\\_melanogaster/cds/Drosophila\\_melanogaster.BDGP6.32.cds.all.fa.gz](http://ftp.ensembl.org/pub/release-103/fasta/drosophila_melanogaster/cds/Drosophila_melanogaster.BDGP6.32.cds.all.fa.gz); Yates et al. 2020). Transcript-level abundance estimates were summarized into gene-level abundance estimates using the release 6.32 version of the *D. melanogaster* gene annotation from Ensembl release 103 ([http://ftp.ensembl.org/pub/release-103/gtf/drosophila\\_melanogaster/Drosophila\\_melanogaster.BDGP6.32.103.gtf.gz](http://ftp.ensembl.org/pub/release-103/gtf/drosophila_melanogaster/Drosophila_melanogaster.BDGP6.32.103.gtf.gz)) using tximport v1.18.0 (Soneson et al. 2015). The summarized gene-level abundance matrix was log-transformed and visualized using the Rtsne package v0.15 (Krijthe 2015) with following parameters: perplexity = 1, theta = 0.0, max\_iter = 5000, check\_duplicates = FALSE.

## Results and discussion

### Clustering of cell lines using TE insertions reveals rare cases of mismatch with expected provenance

We reasoned that TE insertions would be favorable genetic markers for cell line identification in *Drosophila* because the joint processes of germline transposition in whole flies and somatic transposition in cell culture together would create unique TE profiles, both for cell lines derived from distinct *D. melanogaster* donor genotypes and for sublines of cells derived from the same original donor genotype (Figure 1). Furthermore, we posited that shared presence or absence of TE insertions at orthologous loci would allow the identity or similarity among cell line samples to be assessed based on a clustering approach.

We initially investigated the possibility of TE-based cell line identification in *Drosophila* using public genome sequences for 26 samples from 18 cell lines generated by the modENCODE project (Lee et al. 2014; Supplementary Table S1). Paired-end Illumina WGS sequences were used to predict non-reference TEs using TEMP (Zhuang et al. 2014), which showed the least dependence on read length (Supplementary Figure S1) or coverage (Supplementary Figure S2) out of eight non-reference TE detection methods tested on the data used in this study. We clustered cell lines on the basis of their TE profiles using Dollo parsimony, which accounts for the virtually homoplasy-free nature of TE insertions within species (Batzer and Deininger 2002; Ray et al. 2006), the ancestral state of TE absence at individual loci (Batzer and Deininger 2002), and false-negative predictions inherent in non-reference TE detection software (Nelson et al. 2017; Rishishwar et al. 2017; Vendrell-Mir et al. 2019). The use of Dollo parsimony for clustering cell line samples also allows ancestral states to be reconstructed, facilitating inference of which TE families diagnostically identify individual cell lines or groups of cell lines. We note that we do not attempt to interpret the clustering relationships among distinct cell lines in an evolutionary context; however, our approach does provide insight into the evolutionary history of clonally evolving sublines established from the same original cell line.

We predicted between 730 and 2579 non-reference TE insertions in euchromatic regions of *Drosophila* cell line samples from the modENCODE project (Supplementary Table S2). As reported

previously for human cancer cell lines (Zampella et al. 2016), each *Drosophila* cell line sample had a unique profile of TE insertions (Supplementary File S1). The most parsimonious clustering of *Drosophila* cell lines using TE profiles revealed several expected patterns that indicate TE insertions reliably mark the identity of *Drosophila* cell lines (Figure 2A, Supplementary File S2). First, replicate samples of the same cell line cluster most closely with one another with 100% bootstrap support in all seven cases where data are available (S2, S2R+, CME-W1-Cl.8+, ML-DmD9, ML-DmD16-c3, ML-DmD20-c5, and Kc167). Second, different cell lines created in the same lab (presumably from the same ancestral fly genotype) cluster with each other before they cluster with cell lines generated in other labs, or with cell lines having different ancestral genotypes. Third, we observe that divergent sublineages of the same cell line (i.e., S2 and S2R+) cluster closely together (Schneider 1972; Yanagawa et al. 1998). We also find weak evidence for clustering of cell lines generated in different labs (Schneider and Milner) that are derived from the same putative ancestral fly stock (Oregon-R). However, we caution against over-interpretation of this result, given previous reports for substantial genetic diversity among common lab stocks like Oregon-R (Rahman et al. 2015; Stanley and Kulathinal 2016). Also, cell lines derived from the Schneider and Milner labs have distinct BAF profiles, suggesting different ancestral Oregon-R genotypes (Supplementary Figure S3B).

Overall, clustering patterns based on TE profiles suggest that misidentification is rare among the panel of cell lines sequenced by modENCODE. However, we observed two cases where the similarity of cell lines based on genome-wide TE profiles conflicted with expectations based on reported provenance. First, we unexpectedly found that the Sg4 cell line (originally called Sf4 by its maker Donna Arndt-Jovin) clusters most closely with S3 cells, although the DGRC and FlyBase currently consider Sg4 to be a variant of S2 cells (<http://flybase.org/reports/FBBrf0205934.html>; <http://flybase.org/reports/FBtc0000179>; <https://dgrc.bio.indiana.edu/cells/S2isolates>). More strikingly, we also observed that the mbn2 cell line originally reported by Gateff et al. (1980) to be derived from the l(2)mbn stock was placed inside a well-supported cluster containing cell lines (S1, S2, S2R+, S3, and Sg4) generated by Schneider (1972) from an Oregon-R stock. Our clustering of mbn2 cells inside the Schneider cell clade is consistent with a previously unexplained observation that mbn2 cells share an unexpectedly high proportion of TE insertions with both S2 and S2R+ cells (Rahman et al. 2015).

Clarification of the provenance of the Sg4 and mbn2 cell lines used by modENCODE is important since many functional genomics resources were generated for these cell lines (Roy et al. 2010) and over 125 publications involving these cell lines are curated in FlyBase (Larkin et al. 2021). To cross-validate genomic clustering based on TE profiles and to assess potential functional similarity between Sg4↔S3 and mbn2↔S2 cell lines, we clustered cell lines on the basis of their transcriptomes. Transcriptome-based clustering should reveal similarities among cell types rather than genotypes, and thus is not expected to globally match our TE insertion-based clustering. However, both cell type and genotype clustering should support the similarity of pairs of cell lines that are derived from a common ancestral cell line.

Previous transcriptome-based clustering of cell lines based on early whole-genome tiling microarray datasets from the modENCODE project did not reveal similarities among Sg4 and S3 or mbn2 and S2 (Cherbas et al. 2011), however, clustering of small RNA-seq data did reveal similarities among these cell lines (Wen et al. 2014). Using a consistent batch of poly-A RNA-seq samples

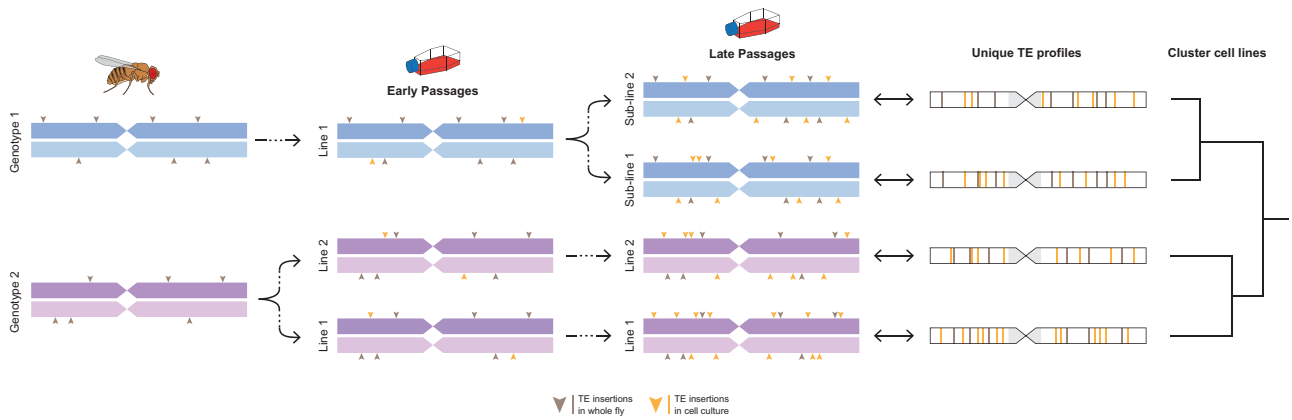


**Figure 1** Germline and somatic transposition jointly can create unique TE profiles in *Drosophila* cell line genomes. A homologous pair of chromosomes is shown for two donor fly genotypes used to establish two distinct cell lines. TE profiles initially differ because transposition events in whole flies (gray arrowheads) are maintained at low population frequencies by purifying selection (Charlesworth and Langley 1989). After the establishment of distinct cell lines, ongoing transposition in cell culture (orange arrowheads) leads to increased TE abundance relative to whole flies (Potter et al. 1979; Ilyin et al. 1980; Rahman et al. 2015) and further differentiates TE profiles, both for distinct cell lines derived from the same or different donor genotypes as well as for sublines of the same cell line. Ultimately, these processes lead to unique TE profiles that can identify cell lines and allow them to be clustered based on shared presence or absence of TE insertions at orthologous loci. The model depicts a simplified case of diploidy, when in reality cell culture genomes can have complex genome structure due to polyploidy and segmental aneuploidy.

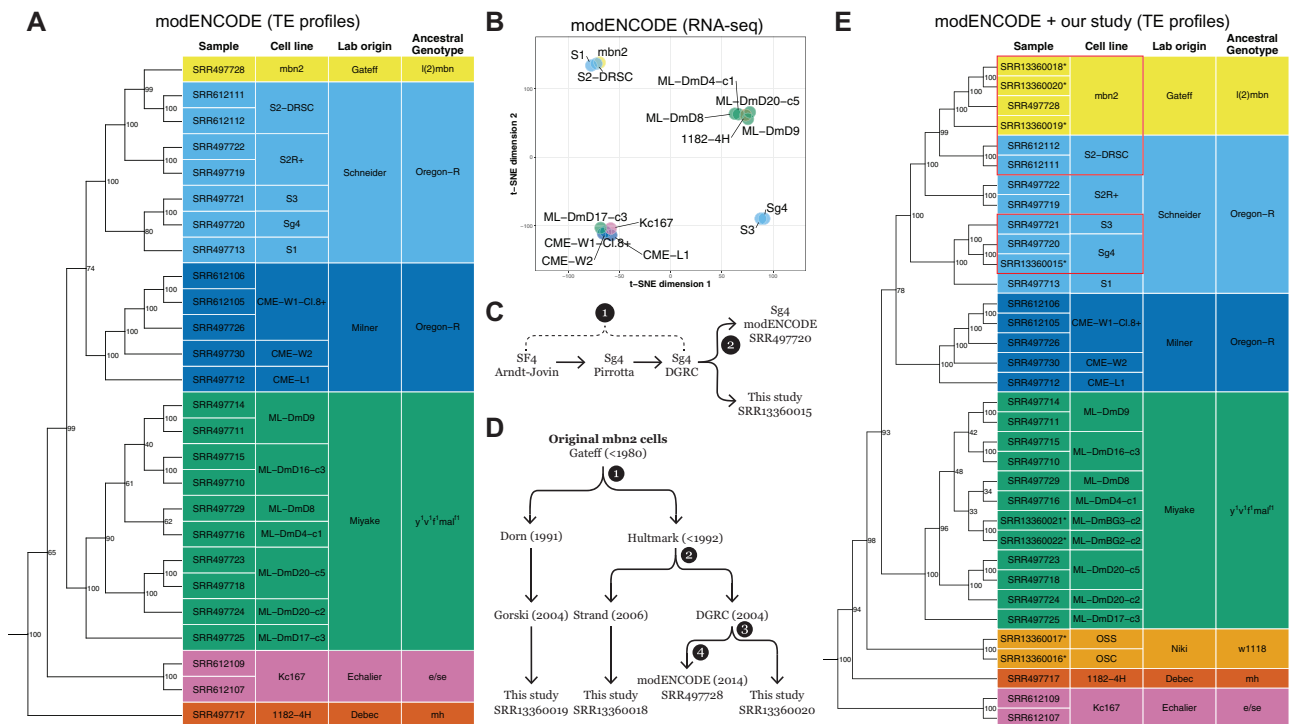


**Figure 2** TE insertion profiles cluster *Drosophila* cell lines by lab origin and reveal unexpected placement of the Sg4 and mbn2 cell lines. (A) Clustering of *Drosophila* cell line samples from the modENCODE project was constructed using Dollo parsimony based on non-reference TE insertions. Samples are colored by the lab origin based on the first publication reporting the original variant of the cell line. Ancestral genotype is based on the *D. melanogaster* stock reported to create the original variant of the cell line. (B) t-SNE visualization of 15 *Drosophila* cell line samples using transcriptomic data in Stoiber et al. (2016). Samples are colored by the lab origin of cell lines. (C) Key events in the history of the Sg4 cell line creation and distribution. (D) Key events in the history of the mbn2 cell line distribution. Node labels in (C) and (D) represent timepoints in the past that potential cell line misidentification events could have occurred. (E) Clustering of *Drosophila* cell line samples from the modENCODE project plus new data reported here (indicated by asterisks in E) was constructed using Dollo parsimony based on non-reference TE insertions. Numbers beside nodes in (A) and (E) indicate percent support based on 100 bootstrap replicates. Red boxes in (E) highlight cases where the reported provenance of *Drosophila* cell lines conflicts with identity inferred from genomic data.

from a panel of 15 DGRC cell lines with genome data (Stoiber et al. 2016; Supplementary Table S3), we estimated expression levels for protein-coding genes then used T-distributed Stochastic Neighbor Embedding (t-SNE) dimensionality reduction (van der Maaten and Hinton 2008; van der Maaten 2014) to

visualize similarity of cell lines based on their gene expression profiles. This analysis revealed that gene expression profiles based on transcriptome data support the clustering of Sg4 with S3 and mbn2 with S2 (Figure 2B). Transcriptome-based clustering of Sg4 with S3 and mbn2 with S2 is also observed in a different

batch of RNA-seq samples generated independently by the modENCODE project (Brown *et al.* 2014; Supplementary Figure S4 and Table S3). These results provide replicated transcriptomic support for the clustering of Sg4↔S3 and mbn2↔S2 cell lines revealed by TE profiles and also highlight functional similarities between these pairs of cell lines.

## TE profiles help resolve the provenance of the Sg4 and mbn2 cell lines

To better understand the cause of the surprising patterns of clustering for the Sg4 and mbn2 cell lines in the modENCODE data, we generated paired-end Illumina WGS sequences for additional samples of Sg4 and mbn2 cells from the DGRC and other sources. In addition, we sequenced several other popular *Drosophila* cell lines (OSS, OSC, ML-DmBG3-c2, and ML-DmBG2-c2) that were not originally sequenced in the modENCODE cell line genome project (Lee *et al.* 2014). To guide sampling and aid the interpretation of the expanded dataset, we reconstructed key events in the history of the Sg4 (Figure 2C) and mbn2 cell lines (Figure 2D). We predicted non-reference TE insertions in these additional samples and then reclustered the expanded dataset using the same methods as the modENCODE-only dataset. The inclusion of additional samples altered some details of the clustering relationships among D-series cell lines generated by the Miyake lab and the position of distantly related cell lines with respect to the root (Kc167 and 1182-4H; Figure 2A vs E). However, key aspects of our clustering approach that facilitate cell line identification (replicates clustering most closely, clustering of cell lines from the same lab/ancestral genotype) appear to be robust to the set of cell line samples analyzed.

Clustering TE profiles from this expanded dataset of 34 samples from 22 *Drosophila* cell lines revealed that our resequenced sample of DGRC Sg4 clusters with high support first with the modENCODE sample of DGRC Sg4 then with S3 (Figure 2E). This result confirms the reproducibility of the S3↔Sg4 genomic similarity and rejects the possibility of cell line swap during the modENCODE cell line sequencing project (node 2; Figure 2C). Additional evidence for the similarity of Sg4 and S3 can be observed in their BAF and CNV profiles. All Sg4 and S3 samples are generally devoid of heterozygosity across their entire genomes, including lacking a small patch of heterozygosity at the base of chromosome arm 2L that is present in all S2 or S2R+ samples (Supplementary Figure S3B). All Sg4 and S3 samples also share CNVs on chromosome arms 2L and 3L that are not present in any S2/S2R+ sample (Supplementary Figure S3C). Together, these data support the conclusion that DGRC Sg4 is a variant of the S3 cell line, not the S2 cell line as currently thought. Presently, we are unable to determine where misidentification of Sg4 as a variant of S2 occurred in the provenance chain from initial development of the cell line by the Arndt-Jovin lab to receipt by the DGRC (node 1; Figure 2C). Future analysis of additional Sg4 sublines circulating in the research community (Morales *et al.* 2004; Schwartz *et al.* 2006) will be necessary to establish the timing of this event and if the S3↔Sg4 similarity first observed in the DGRC Sg4 subline is more widespread.

The second case of unexpected clustering we observed in the modENCODE data involving mbn2 and S2 is potentially more surprising and consequential given that these cell lines are reported to be derived from different ancestral genotypes. mbn2 cells were reportedly derived from a stock carrying l(2)mbn on a 2nd chromosome marked with three visible mutations (Gateff 1977; Gateff *et al.* 1980), while S2 cells were derived from a wild-type Oregon-R stock (Schneider 1972). Unfortunately, the l(2)mbn mutation was

never characterized at the molecular level, and no fly stocks carrying l(2)mbn currently exist in public stock centers that could be sequenced and compared with the mbn2 cell line. In the absence of external biological resources to verify the identity of an authentic mbn2 cell line, we attempted to infer the timing and extent of the potential mbn2 misidentification event first observed in the modENCODE data by sequencing sublines of mbn2 from DGRC and other sources. We resequenced another sample of the DGRC mbn2 subline, a subline from the Strand lab (University of Georgia) derived from the same donor as the DGRC subline (Hultmark lab, Umeå University), and a subline from the Gorski lab (Canada's Michael Smith Genome Sciences Centre, BC Cancer) derived from an independent donor (Dorn lab, Johannes Gutenberg-Universität Mainz; Figure 2D). The Hultmark and Dorn labs each report obtaining mbn2 cells directly from the Gateff lab in the early 1990s (Samakovlis *et al.* 1992; Ress *et al.* 2000). This sampling allowed us to infer if potential misidentification occurred during the modENCODE project (node 4), at the DGRC (node 3), in the Hultmark lab (node 2) or in the Gateff lab (node 1; Figure 2D).

Analysis of TE profiles in our expanded dataset revealed that all four samples of mbn2 cluster together as a single, well-supported group that is most similar to a cluster containing S2 cells (Figure 2E). The detailed relationships among sublines within the mbn2 cluster deviate slightly from expectations based on cell line history (Figure 2D); however, this discrepancy appears to be caused by differences in read length or coverage between the data from modENCODE and our study (Supplementary Figure S5). All mbn2 samples have the low SNP heterozygosity across most of their genomes that is characteristic of Schneider cell lines, and also share the small patch of heterozygosity at the base of chromosome arm 2L found in S2 and S2R+ cells (Supplementary Figure S3B). Additionally, all four mbn2 samples share widespread segmental aneuploidy across the entire euchromatin that is a common hallmark of S2 and S2R+ cells, but not other *Drosophila* cell lines (Supplementary Figure S3C). Together, these data support the conclusions that multiple independent sublines of mbn2 cells all share a common origin and are likely to descend from a single divergent lineage of S2 cells. Based on these observations, we speculate that currently circulating mbn2 cells derive from a mislabeling or cross-contamination event with S2 cells in the Gateff lab that occurred prior to distribution to the Hultmark or Dorn labs (node 4; Figure 2D). This scenario is consistent with the facts that S2 cells were developed and widely distributed prior to the origin of mbn2 cells (Schneider 1972; Gateff *et al.* 1980) and that there was a 12-year gap between the initial report describing mbn2 cells and use in any subsequent publication (Gateff *et al.* 1980; Samakovlis *et al.* 1992).

The possibility that mbn2 is a divergent lineage of S2 is plausible given that both cell lines are thought to have a hemocyte-like cell type (Gateff *et al.* 1980; Cherbas *et al.* 2011; Luhur *et al.* 2019). Furthermore, it is known that different lineages of *bona fide* S2 cells vary substantially in their morphology and gene expression, some of which share properties with mbn2 cells (Samakovlis *et al.* 1992; Yanagawa *et al.* 1998; Cherbas *et al.* 2011; Supplementary Figure S6). Under phase-contrast microscopy, canonical S2 cells represented by the S2-DRSC subline are generally a mix of loosely adherent spherical cells and simple round flat cells. In contrast, live S2R+ cells can be characterized by many “phase dark” cells that attach to the growth substrate, which can flatten out to exhibit both polygonal and “fried egg” morphology. S2R+ cells that are loosely attached to the growth surface are generally spherical

with fine cell protrusions. Like S2R+ cells, *mbn2* cells are characterized by a mix of flattened phase dark cells that assume the polygonal and fried egg morphology, as well as loosely adhering spherical cells. However, loosely adherent *mbn2* cells have a bigger diameter relative to S2-DRSC and S2R+ cells. Recognition of *mbn2* as a potentially divergent S2 lineage suggests that there is more phenotypic diversity among different S2 lineages than previously thought.

### A subset of LTR retrotransposon families are sufficient to identify *Drosophila* cell lines

Our analysis has thus far provided evidence that TE insertion profiles of commonly used *Drosophila* cell lines based on whole-genome sequences can be used to cluster cell lines and uncover cases of cell line misidentification. However, for these results to form the foundation for a *Drosophila* cell line authentication protocol, it is necessary to show that a cell line sample can successfully be identified on the basis of its TE profile. Furthermore, it is important to explore if whole-genome data are required for TE-based cell line identification in *Drosophila* since the cost of WGS could preclude its routine application by many labs. Therefore, we next investigated whether a subset of *Drosophila* TE families could potentially be sufficient for *Drosophila* cell line identification, with the aim of guiding the development of a cost-effective targeted PCR-based enrichment protocol that could be used more widely by the research community.

To investigate this possibility, we first clustered a non-redundant dataset of one “primary” replicate from each of the 22 *Drosophila* cell lines in the expanded dataset based on their whole-genome TE profiles (Figure 3A), which resulted in a similar clustering to the same sample of 22 cell lines including all replicates (Figure 2E). Replicates with the longest read length or depth of coverage were chosen as the primary replicate in the non-redundant dataset (Supplementary Table S1). We then took advantage of the ability of Dollo parsimony to reconstruct ancestral states and map the gain of TE insertions on each branch of the most parsimonious tree. TE insertions were then aggregated into families on each branch of the tree to visualize family- and branch-specific TE insertion profiles. This analysis revealed that a subset of 60 out of the 125 curated TE families in *D. melanogaster* are informative for *Drosophila* cell line clustering using TEMP predictions (Figure 3B, Supplementary File S3). Within the set of clustering-informative TE families, we observed that some TE families are broadly represented across many cell lines with different origins (e.g., *copia*, 297, *jockey*, *mdg3*, *mdg1*, and *roo*), although the quantitative abundance of these TE families varies across cell lines. Other TE families appear to be represented in only one cell line or a subset of cell lines from the same lab origin (e.g., ZAM, Tabor, HMS-Beagle2, *gypsy5*, 1731, 17.6, *springer*, Tirant, rover, and *micropia*). These results provide systematic genome-wide evidence for the classical observation that proliferation of different TE families in cultured *Drosophila* cells is cell-line dependent (Echalier 1997). Additionally, these patterns of cell-line-specific TE proliferation provide further support for the conclusions that the DGRC Sg4 cell line is a lineage of S3 cells (all share *Ivk* proliferation), and that *mbn2* cell lines are a divergent lineage of S2 cells (all share 1731 proliferation; Figure 3B).

Based on these results, we next evaluated whether a small, experimentally tractable subset of TE families is sufficient to cluster and identify *Drosophila* cell lines. For this analysis, we focused on LTR retrotransposon families since this type of TE inserts with intact termini and therefore provide reliable 5' and 3' junctions for targeted PCR-based enrichment protocols (Smukowski Heil

et al. 2021). We used the pattern of family- and branch-specific TE insertion to heuristically guide the selection of a subset of six LTR retrotransposon families (*copia*, 297, *mdg3*, *mdg1*, *roo*, and 1731; TE family names highlighted in red in Figure 3B), which defined unique TE profiles for each cell line and generated the same major patterns of *Drosophila* cell line clustering as the genome-wide dataset of all 125 TE families (Figure 3C). Finally, we tested whether a cell line sample (not used in the tree construction) can be accurately identified on the basis of its six-family TE profile. To do this, we used the six-family TE tree derived from the non-redundant set of primary replicates as a backbone to constrain Dollo parsimony searches including one additional “secondary” replicate for each of the 12 secondary replicates from the nine cell lines in the expanded dataset with secondary replicates. In 100% of cases (12/12), the additional secondary replicate clustered most closely with the primary replicate from the same cell line (Supplementary Figure S7). In 10/12 cases, the bootstrap support for the clustering of replicates was 100%, and the remaining two cases (both for CME-W1-Cl.8+) had lower bootstraps ( $\geq 64\%$ ) presumably because of the short-read length for these secondary replicates (50 bp). This proof-of-principle analysis indicates that TE insertions from a small subset of LTR retrotransposon families can accurately identify *Drosophila* cell line samples, and that only a subset of “diagnostic” TE families are needed to develop a *Drosophila* cell line authentication protocol. Based on these results, we have developed and validated a PCR enrichment-based NGS protocol that generates genome-wide TE profiles using this subset of LTR retrotransposon families and can be used to authenticate *Drosophila* cell lines at lower cost than WGS analysis (D. Mariyappa, D.B. Rusch, S. Han, A. Luhur, D. Overton, D.F.B. Miller, C.M. Bergman, A.C. Zehlf, unpublished results).

### TE profiles provide insight into *Drosophila* ovarian cell line history

The observation that different TE families are amplified in distinct *Drosophila* cell lines raises the question of whether a single TE family could diagnostically mark the identity of a *Drosophila* cell line or subline. One such candidate for this possibility is the retroviral-like LTR retrotransposon ZAM in the closely related OSS and OSC ovarian somatic cell lines (Niki et al. 2006; Saito et al. 2009). As shown above, we observed a massive increase in ZAM insertions in OSS cells relative to the OSC cell line (branches 19 and 20 in Figure 3, A and B), supporting previous findings by Sytnikova et al. (2014). However, Sytnikova et al. (2014) also reported that ZAM amplification did not occur in all OSS sublines, only in a contemporary subline of OSS cells (called OSS\_C), but not in a putatively early passage subline of OSS cells (called OSS\_E).

To address whether ZAM proliferation is restricted to a subset of OSS sublines or is in fact a specific marker for all OSS sublines, we performed an integrated analysis of TE predictions in WGS data from six OSS and OSC samples from our and two previous studies (Sienski et al. 2012; Sytnikova et al. 2014). To formulate alternative hypotheses and guide interpretation of our results, we first compiled the reported provenance of these six OSS and OSC cell line samples. As shown in Figure 4A, the ultimate ancestor of all OSS and OSC cell lines is a cell line composed of germline and somatic ovarian cell types called fGS/OSS (Niki et al. 2006). fGS/OSS cells were subsequently selected in the Niki lab to remove germline-marked stem cells to create the ancestor of the OSS (ovarian somatic sheet) cell line. The Niki lab sent two batches of OSS cells to the Lau lab in 2007 (N. Lau, personal communication): one was expanded and continuously cultured to become

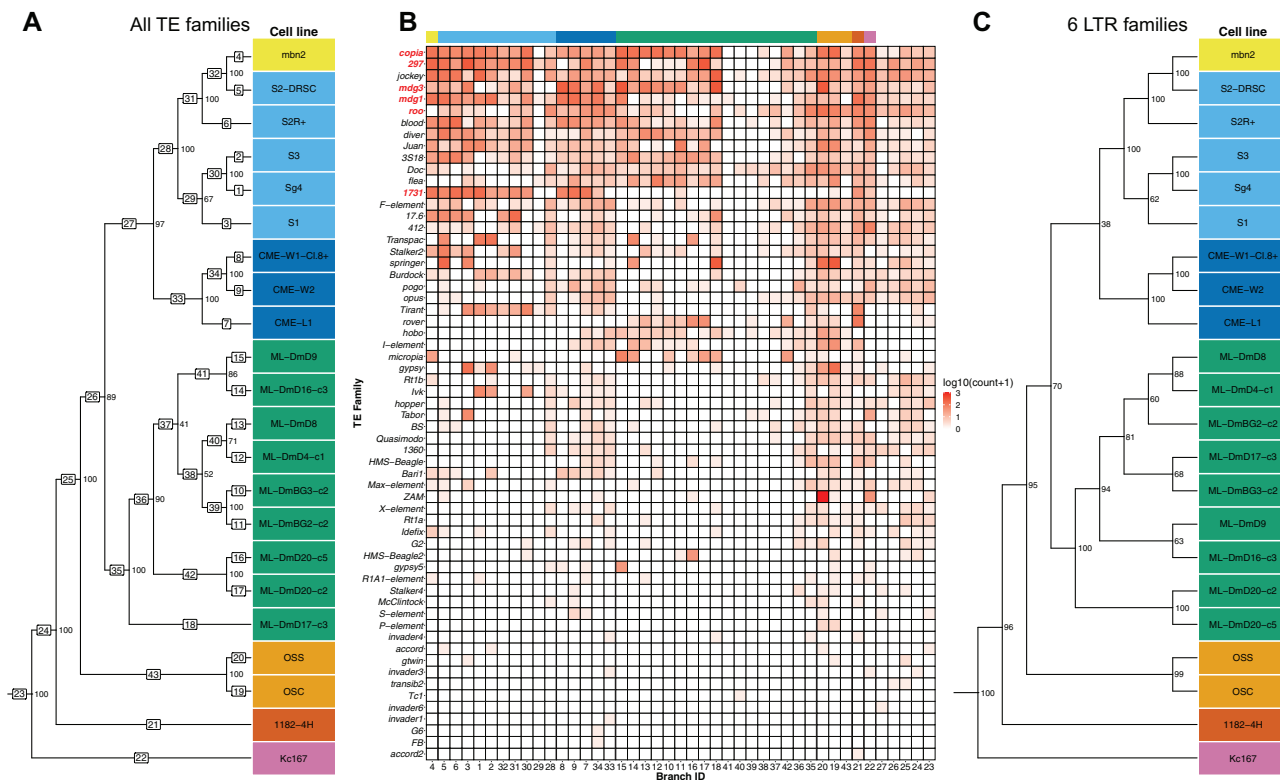


**Figure 3** A small subset of LTR retrotransposon families can identify *Drosophila* cell lines. (A) Dollo parsimony tree of 22 *Drosophila* cell lines (without replicates) based on non-reference TE predictions for all 125 *D. melanogaster* TE families. Samples are colored by lab origin as in Figure 2. Numbers inside boxes on branches indicate branch ID, and numbers beside nodes indicate percent support based on 100 bootstrap replicates. (B) Heatmap showing the number of non-reference TE insertion gain events per family on each branch of the tree in (A) based on ancestral state reconstruction using Dollo parsimony. The heatmap is colored by log-transformed [ $\log_{10}(\text{count} + 1)$ ] number of gains per family per branch, sorted top to bottom by overall non-reference TE insertion gains per family across all branches, and sorted left to right into clades representing lab origin with lab origin color codes indicated at the top of the heatmap. The six diagnostic LTR retrotransposon families used in (C) are highlighted in red. (C) Dollo parsimony tree of 22 *Drosophila* cell lines (without replicates) based on non-reference predictions of six LTR retrotransposon families (297, copia, mdg3, mdg1, roo, and 1731). Numbers beside nodes indicate percent support based on 100 bootstrap replicates.

the OSS\_C subline; the other was briefly cultured and stored as a cryopreserved culture for many years, then thawed and sequenced in 2013 creating the OSS\_E sample (Sytnikova et al. 2014). Our sample of OSS cells comes from an independent subline donated by the Niki lab to the DGRC in 2010 (OSS\_DGRC). The Niki lab also sent FGS/OSS cells to the Siomi lab, who independently selected against germline cells to create another somatic cell line called OSC (ovarian somatic cells; Saito et al. 2009). OSC cells were sent by the Siomi lab in 2010 separately to the Lau (OSC\_C) and Brennecke (OSC\_E) labs and were later donated by the Siomi lab to the DGRC in 2019 (OSC\_DGRC).

Because WGS data from Sienski et al. (2012) and Sytnikova et al. (2014) is single-ended, integrated analysis of ovarian cell lines required a different TE prediction strategy than the one used for the analysis of the paired-end datasets above. Preliminary analyses revealed that some single-end TE predictors (e.g., ngs\_te\_mapper, RelocaTE; Linheiro and Bergman 2012; Robb et al. 2013) severely under-predicted insertions specifically for the ZAM family in the DGRC OSS sample relative to TEMP results based on paired-end data (Supplementary Figure S8). Additionally, our analysis of OSS and OSC samples ultimately required tracking intra-sample TE allele frequencies, which is not available in other TE predictors that use single-end data (e.g., TIDAL; Rahman et al. 2015). Thus, we developed a new implementation of the single-end TE predictor originally described in Linheiro and Bergman (2012) called ngs\_te\_mapper2 ([https://github.com/bergmanlab/ngs\\_te\\_mapper2](https://github.com/bergmanlab/ngs_te_mapper2)) that improves speed

and sensitivity relative to the original version and has been extended to estimate intra-sample TE allele frequencies (Supplementary Figure S9 and Tables S4 and S5; see Supplementary Text for details).

Using datasets normalized to the same read length and coverage in order to optimize the resolution of closely related sublines, we predicted non-reference TE insertions in all OSS and OSC sublines with ngs\_te\_mapper2 (Supplementary File S4). These results revealed that ZAM has proliferated massively in the OSS\_DGRC and OSS\_C sublines (553 and 630 copies, respectively, in euchromatic regions), but is present in only one or two copies in OSS\_E and all OSC sublines (Figure 4B). The abundance of ZAM in these ovarian cell lines is more than 10-fold higher than fly strains where ZAM has been mobilized because of deletions in the *flamenco* piRNA locus (Leblanc et al. 1999; Zanni et al. 2013) or because of multigenerational knockdown of the piRNA effector protein piwi (Barckmann et al. 2018; Mohamed et al. 2020).

Under the “reported provenance” hypothesis that OSS\_E and OSS\_C share a more recent common ancestor than they do with OSS\_DGRC (branch 1; Figure 4A), this pattern of ZAM abundance can only be explained by unlikely scenarios such as a massive loss of ZAM insertions on the branch leading to OSS\_E, or independent parallel amplifications of ZAM on the OSS\_C and OSS\_DGRC sublines. An alternative hypothesis to explain the pattern of ZAM abundance is motivated by another observation made by Sytnikova et al. (2014): OSS\_E shares more TE insertions in common with OSC sublines (OSC\_E and OSC\_C) than it does



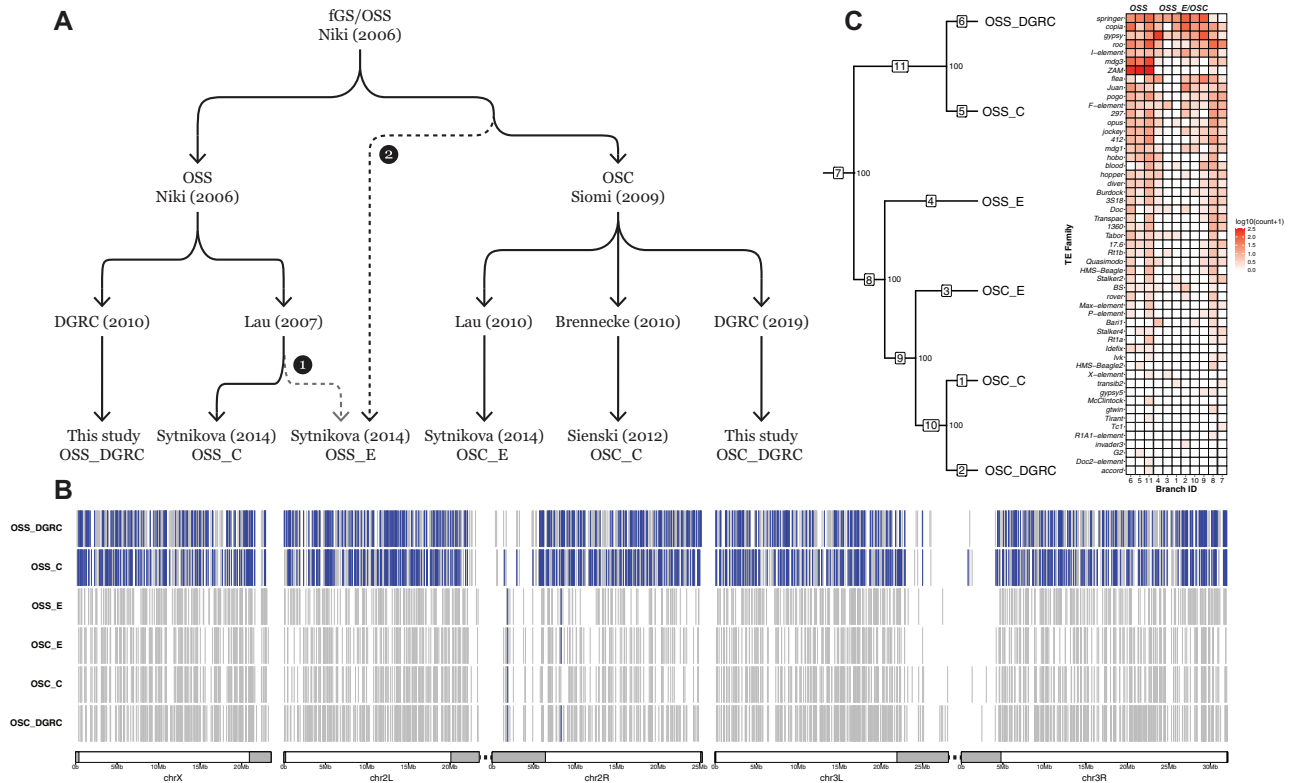


**Figure 4** ZAM proliferation reveals OSS cell line identity. (A) Key events in the history of OSS and OSC cell line creation and distribution. Dotted lines represent alternative hypotheses for the identity of OSS\_E. Branch 1 represents the reported provenance that hypothesizes OSS\_E is an early-diverging OSS subline; branch 2 hypothesizes that OSS\_E approximates an ancestral state of the OSC cell line. (B) Genome-wide non-reference TE insertion data for six ovarian cell lines with ZAM insertions highlighted in blue and all other TE families in gray. (C) Dollo parsimony tree of ovarian cell lines based on all non-reference TE predictions. Numbers inside boxes on branches indicate branch ID, and numbers beside nodes indicate percent support based on 100 bootstrap replicates. (Left) Heatmap showing the number of non-reference TE insertion gain events per family on each branch of the tree based on ancestral state reconstruction using Dollo parsimony. The heatmap is colored by log-transformed [ $\log_{10}(\text{count} + 1)$ ] number of gains per family per branch, sorted top to bottom by overall non-reference TE insertion gains per family across all branches and sorted left to right into the *bona fide* OSS and OSS\_E/OSC clusters (right).

with a contemporary OSS subline (OSS\_C). This pattern is not expected under the reported provenance hypothesis and suggests that OSS\_E may in fact be an OSC-like lineage, rather than an early passage OSS subline. Under this alternative “uncertain provenance” hypothesis (branch 2; Figure 4A), the only *bona fide* OSS sublines would be OSS\_C and OSS\_DGRC, and ZAM proliferation could truly be a diagnostic marker of OSS cell line identity.

To test these alternative hypotheses, we used *ngs\_te\_mapper2* predictions as input to cluster OSS and OSC sublines using Dollo parsimony. We found two highly supported clusters, one containing only the OSS\_C plus OSS\_DGRC sublines and the other containing OSS\_E plus all OSC sublines (Figure 4C, Supplementary File S5). Ancestral state reconstruction clearly demonstrated that high ZAM abundance is restricted to the cluster containing OSS\_C and OSS\_DGRC sublines. The only two ZAM insertions that are found in OSS\_E and OSC sublines are both shared by multiple sublines and therefore likely inserted in a common ancestor of the entire clade (Figure 4B, Supplementary File S6). We verified that the clustering relationships among OSS and OSC sublines were not solely driven by the ZAM amplification by repeating our clustering analysis excluding ZAM insertions, obtaining the same topology as in the complete dataset (Supplementary Figure S11A).

Further support for the hypothesis that OSS\_E is an OSC-like lineage can be found in patterns of SNP and CNV variation in these cell line genomes (Supplementary Figure S11, B and C).

OSS\_C and OSS\_DGRC have essentially identical BAF profiles across the entire genome (Supplementary Figure S11B). In contrast, OSS\_E and OSC sublines share a BAF profile everywhere but the distal regions on chromosome arms 2L, 3L, and 3R (Supplementary Figure S11B, Figure 5A). BAF profiles on all of chromosome X and arm 2R clearly differentiate OSS\_C and OSS\_DGRC (heterozygous) from OSS\_E and OSC sublines (homozygous; Supplementary Figure S11B). Likewise, CNV profiles support the clustering of OSS\_C with OSS\_DGRC, and OSS\_E with the OSC sublines. OSS\_C and OSS\_DGRC share a large deletion on chromosome X not found in OSS\_E plus OSC sublines, and OSS\_E plus the OSC sublines share a smaller deletion on chromosome arm 3L not found in OSS\_C or OSS\_DGRC (Supplementary Figure S11C). Based on these results, we conclude that OSS\_E is a divergent lineage of OSC cells rather than early passage OSS cells, that ZAM amplification truly marks *bona fide* OSS cell lines (include the OSS line distributed by the DGRC), and that *ngs\_te\_mapper2* TE predictions based on single-end WGS data can be effectively used to cluster *Drosophila* cell lines and reveal aspects of cell line history.

### Loss of heterozygosity impacts TE profiles in *Drosophila* cell culture

Reinterpreting OSS\_E as a divergent lineage of OSC cells requires explaining both the similarity and distinctness of its TE, BAF, and CNV profiles from other OSC sublines. Two observations led us to

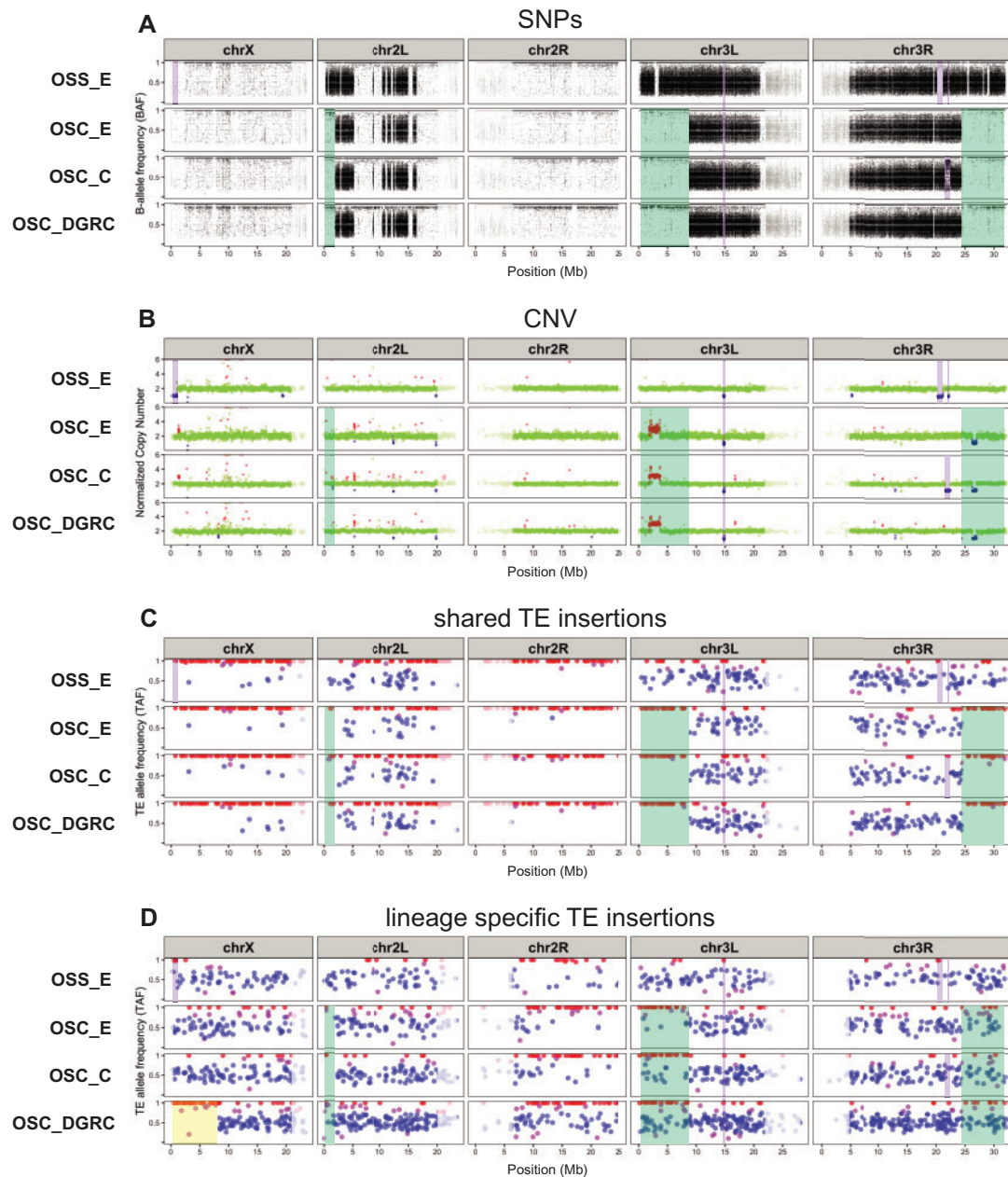


**Figure 5** LOH, copy number evolution, and ongoing transposition shape TE profiles in *Drosophila* ovarian somatic cell lines. Genome-wide profiles for OSS\_E and OSC sublines of (A) intra-sample allele frequency based on SNP variants, (B) copy number, (C) intra-sample allele frequency based on TE insertions shared by OSS\_E and OSC sublines, and (D) intra-sample allele frequency based on lineage-specific TE insertions restricted to only OSS\_E or the OSC sublines. SNPs and TE insertions in highly repetitive low recombination regions are shaded in grey. For SNP profiles, the BAF was determined as the coverage of reads supporting the non-reference allele divided by total coverage at that variant positions; regions of heterozygosity in a diploid genome are shown in BAF profiles where clusters of SNPs have allele frequencies centered around 0.5. For copy number profiles, each data point represents normalized copy number (ratio\*ploidy) for a given 10-kb window estimated by Control-FREEC (Boeva et al. 2012); data points for each window are colored by CNV status (red: CNV gain; green: no CNV; blue: CNV loss), which are based on the comparison between normalized copy number for that window and a baseline ploidy of  $2n$ . For TE profiles, TE insertions are classified as being homozygous (red), heterozygous (blue), or undefined (purple) based on intra-sample allele frequencies estimated by ngs\_te\_mapper2. Green shading indicates copy-neutral LOH regions defined by more extensive patterns of SNP heterozygosity in OSS\_E relative to OSC sublines that are putatively caused by mitotic recombination. Yellow shading indicates copy-neutral LOH regions based on runs of homozygous TE insertions in OSC\_DGRC relative to other OSC sublines that are putatively caused by mitotic recombination. Purple shading indicates LOH regions that are putatively caused by segmental deletion.

hypothesize that OSS\_E approximates an ancestral state of current OSC sublines. First, OSS\_E occupies a basal position in the OSS\_E plus OSC cluster based on TE profiles (Figure 4C). Second, the BAF profile for OSS\_E shows heterozygosity that extends in the distal regions of chromosome arms 2L, 3L, and 3R relative to OSC sublines (green shading, Figure 5A). We propose that

differences in BAF profiles in these distal regions are caused by LOH that occurred in an ancestor of all OSC sublines after divergence from the lineage leading to OSS\_E. We infer that these large-scale distal LOH events were caused by a copy-neutral process such as mitotic recombination, since the baseline copy number in these distal LOH regions is the same in OSS\_E and OSC

sublines (Figure 5B, Supplementary Figure S11C). Similar to previous reports in a primate cell line (Osada et al. 2014), we do observe smaller copy number gain and loss events, respectively, within the large regions of LOH on chromosome arms 2L and 3R. However, these copy number events are much smaller and fully contained within the larger LOH regions and therefore unlikely to be the cause of the large-scale distal LOH events. Despite previous evidence for putatively polyploid cells in the OSS\_E subline (Sytnikova et al. 2014), we infer a diploid baseline copy number in the “stem line” that leads to the majority of inherited cells in the OSS\_E and OSC sublines, since BAF profiles (Figure 5A) and DNA density profiles (Supplementary Figure S10) of the bulk samples show modal values that together are consistent with diploidy but not any higher ploidy values.

If this evolutionary scenario is correct, shared TEs (which inserted prior to the divergence of OSS\_E and OSC sublines) that are heterozygous in OSS\_E are predicted to be homozygous in OSC sublines in distal LOH regions, but should maintain heterozygosity elsewhere in the genome. To test these predictions, we used intra-sample allele frequency estimates from *ngs\_te\_mapper2* to classify the zygosity of TE insertions in OSS\_E and OSC sublines. Evaluation of our classifier on simulated diploid genomes revealed it had >91% precision and crucially never falsely classified heterozygous insertions as homozygous (Supplementary Table S6), and is thus conservative with respect to detection of LOH using TE insertions. As predicted under our model, we observed that there are many shared TE insertions in distal LOH regions that are heterozygous in OSS\_E but virtually all TE insertions in these regions are homozygous in OSC sublines (green shading, Figure 5C). Outside of distal LOH regions, shared TE insertions that are heterozygous in OSS\_E generally retain heterozygosity in OSC sublines (Figure 5C). In contrast, we observe that many lineage-specific TE insertions (which occurred after the divergence of OSS\_E and OSC sublines) are heterozygous in OSC sublines in distal LOH regions (green shading, Figure 5D). Together these results support the inferences that OSS\_E approximates an ancestral state of current OSC sublines, that LOH events can cause fixation of previously heterozygous TE insertions in *Drosophila* cell lines, and that ongoing transposition in *Drosophila* cell culture can restore genetic variation in regions where previous large-scale LOH events have eliminated ancestral SNP or TE insertion variation.

Contrasting patterns of genetic variation between OSS\_E and OSC sublines in distal regions of chromosome arms 2L, 3L, and 3R provided the initial evidence for LOH as mechanism of genome evolution in *Drosophila* cell culture. Additional evidence for copy-neutral LOH in *Drosophila* cell culture can be found in the lack of SNP heterozygosity on all of chromosome X and arm 2R (Figure 5A), which can be explained by whole-arm LOH events caused by centromere-proximal somatic recombination events in the common ancestor of the OSS\_E/OSC lineage, assuming that the genome-wide heterozygosity observed in *bona fide* OSS sublines is ancestral (Supplementary Figure S11B). Consistent with the prediction of whole-arm LOH in the ancestor of the OSS\_E/OSC lineage followed by ongoing transposition in cell culture, we observe that most shared TE insertions on chromosome X and arm 2R are homozygous (Figure 5C), while lineage-specific TE insertions are heterozygous (Figure 5D). Intriguingly, and in contrast to other OSC sublines, we also observe that lineage-specific TE insertions on the distal eight megabases of chromosome X in OSC\_DGRC are almost all homozygous (yellow shading, Figure 5D). This observation can be explained by a secondary copy-neutral LOH event in the distal region of chromosome X that

occurred recently only in the OSC\_DGRC lineage. In this case, heterozygosity restored by ongoing TE insertion in *Drosophila* cell culture allows detection of subsequent LOH events in the same genomic region that cannot be detected using SNP variation.

In addition to large-scale LOH events affecting distal regions or whole chromosome arms that can be explained by copy-neutral processes such as mitotic recombination, we also observed smaller-scale LOH events that can be explained by hemizygosity due to segmental deletion (purple shading, Figure 5, A and B). For example, we observe a 200-kb region on chromosome arm 3L in all OSS\_E and OSC sublines that lacks heterozygous SNPs which can be explained by a segmental deletion that occurred in the common ancestor of the OSS\_E/OSC lineage (Figure 5, Supplementary Figure S12). LOH by segmental deletion is supported by shared TEs in this region being homozygous in all OSS\_E and OSC sublines. Likewise, in OSS\_E, we observe two subline-specific segmental deletions on chromosome arm 3R of 900 and 100 kb, respectively that lack heterozygous SNPs and TE insertions in the corresponding regions (Figure 5, Supplementary Figure S12). We also observe a subline-specific segmental deletion on chromosome arm 3R of 800 kb in OSC\_C that exhibits a BAF profile enriched at 0.85 (Figure 5, Supplementary Figure S12) rather than the homozygosity expected for complete LOH due to hemizygosity. Similar to patterns of LOH in mammalian tumors that have incomplete purity (Song et al. 2012), we interpret the incomplete LOH in this region as being caused by clonal heterogeneity in the OSC\_C subline, with the majority of cells having the segmental deletion but a small proportion of cells lacking it. If this hypothesis is correct, the median copy number should be slightly over 1 in the segmentally deleted LOH region in OSC\_C: as predicted, the median copy number of OSC\_C in the putative LOH region is 1.14 (Supplementary Figure S12). Additionally, the OSS\_E subline also exhibits a terminal deletion on the tip of chromosome X (Figure 5, Supplementary Figure S12), which does not lead to LOH in the SNP profile because of the primary whole-arm LOH event proposed to have occurred in the ancestor of the OSS\_E/OSC lineage. However, similar to the secondary LOH event proposed to have occurred by somatic recombination on the distal region of chromosome X in OSC\_DGRC, recovery of heterozygosity by ongoing TE insertion allows secondary LOH by segmental deletion to be observed in the lineage-specific TE-allele frequency (TAF) profile at the tip of chromosome X in OSS\_E. Finally, we note that LOH events that can be explained by segmental deletions provide further support for a diploid stem line in the OSS\_E/OSC lineage, since hemizygosity in a diploid is more parsimonious than scenarios such as multiple identical deletions or deletions followed by mitotic recombination required to explain LOH by segmental deletion in genomes with higher ploidies.

As LOH has not previously been reported as a mechanism of genome evolution in *Drosophila* cell culture, we sought to find additional evidence for this process by inspecting BAF profiles for other *Drosophila* cell lines in the expanded dataset. This led us to additional evidence for large-scale LOH events defined by SNPs on chromosome arms 2R and 3L of the CME-W2 and CME-W1-CI.8+ cell lines (Supplementary Figures S3B and S13A), both of which are reported to have a diploid baseline autosomal copy number (Lee et al. 2014). As with OSS\_E, we propose that the more extensive heterozygous BAF profile on these chromosome arms in CME-W2 represents the pre-LOH ancestral-like state, and the homozygous BAF profile of CME-W1-CI.8+ represents the post-LOH derived state. This scenario is consistent with the reported establishment of CME-W1-CI.8+ from a single cloned cell of a polyclonal cell line (CME-W1) with the same ancestral genotype

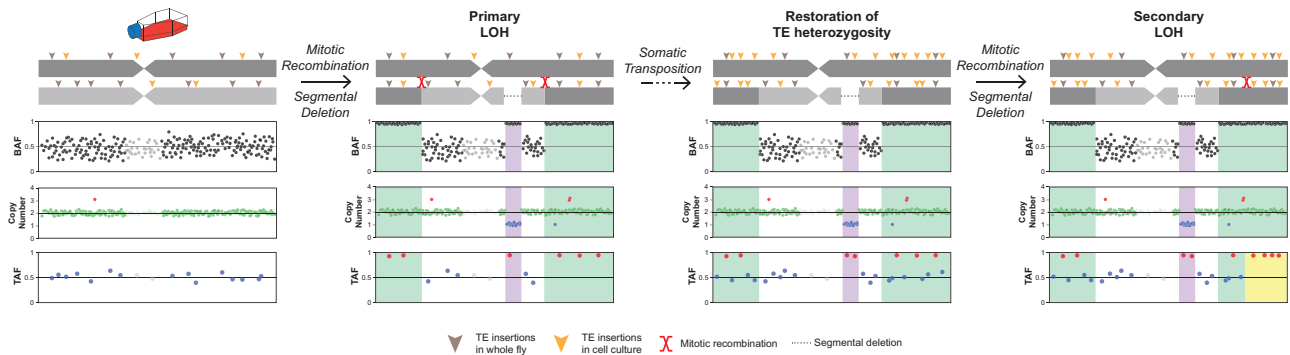


**Figure 6** Schematic model of how LOH and somatic transposition interact to shape TE profiles in diploid *Drosophila* cell line genomes. Mitotic recombination (green shading) or segmental deletion (purple shading) can cause LOH of pre-existing heterozygous SNP and TE variants, as revealed by changes in BAF and TAF profiles. Ongoing transposition in cell culture leads to the accumulation of new haplotype-specific heterozygous TE insertions inside and outside of primary LOH regions. Recovery of TE heterozygosity allows detection of secondary LOH events (yellow shading) in regions of the genome that have previously undergone primary LOH events. Secondary LOH can occur by either mitotic recombination or segmental deletion, but only mitotic recombination is depicted here. We note that this model depicts a simplified case of diploidy which applies to some cell lines such as the OSS\_E/OSC and CME-W2/CME-W1-Cl.8+ lineages, however, many cell culture genomes can have complex genome structure due to polyploidy and aneuploidy.

as CME-W2 (Currie et al. 1988; Peel and Milner 1990). The lack of difference in the baseline copy number profiles on chromosome arms 2R and 3L of CME-W2 and CME-W1-Cl.8+ suggests these large-scale LOH events were also due to mitotic recombination (Supplementary Figure S13B). As predicted under the LOH model, we observed many TE insertions shared by CME-W2 and CME-W1-Cl.8+ are heterozygous in CME-W2 but are nearly all homozygous in CME-W1-Cl.8+ in LOH regions (Supplementary Figure S13C). Like in OSC sublines, we also observed many heterozygous TE insertions that are specific to CME-W1-Cl.8+ in LOH regions (Supplementary Figure S13D), consistent with recovery of TE insertion variation after LOH. Similar to the OSS\_E/OSC lineage, we also find evidence in the CME-W2/CME-W1-Cl.8+ lineage for smaller-scale LOH events on chromosome arm 3R that can be explained by segmental deletion (Supplementary Figures S13 and S14), with clonal heterogeneity explaining incomplete LOH by segmental deletion at the tip of chromosome arm 3R in CME-W2. Finding evidence for both mechanisms of LOH in distinct cell lineages developed in different labs generalizes the inference that LOH shapes TE profiles in *Drosophila* cell lines and suggests that LOH in *Drosophila* culture is not dependent on the genetic background of the ancestral fly donor.

## Conclusions

Here, we demonstrate that TE insertion profiles can successfully identify *Drosophila* cell lines and use this finding to clarify several aspects of cell line provenance in *Drosophila*. The success of this approach validates our basic model for how the joint processes of germline transposition in whole flies and somatic transposition in cell culture create TE profiles that uniquely mark *Drosophila* cell lines (Figure 1). We also show that TE insertion profiles can shed light on the evolutionary history of *Drosophila* cell lines derived from a common ancestral cell line and that LOH is an additional mechanism of genome evolution in cell culture that adds complexity to our basic model (Figure 6). During cell culture, LOH resulting from mitotic recombination (green shading) or segmental deletion (purple shading) purges ancestral variation and causes previously heterozygous SNPs and TE insertions to become fixed or lost within a cell line genome. Ongoing transposition in cell culture leads to the relatively rapid recovery of TE but not SNP heterozygosity, allowing

secondary LOH events to be identified using TE insertions in regions that have previously lost ancestral variation due to primary LOH events (yellow shading). The emerging model of TE evolution in cell culture motivated by results presented here has direct implications for the development of protocols for cell line identification in *Drosophila* and contributes to our general understanding of the mechanisms of genome evolution in cell lines derived from multicellular organisms.

## Data availability

Raw sequencing data generated in our study are available in the SRA under BioProject PRJNA689777. Supplementary material is available at figshare: <https://doi.org/10.25386/genetics.14884977>. Supplementary File S1 contains non-redundant bed files from McClintock runs using TEMP module on the expanded dataset including 34 *Drosophila* cell line samples (reference TEs, INE-1 insertions, and TEs in low recombination regions excluded). Supplementary File S2 contains clustered TE profiles in the format of binary presence/absence data matrix including 34 *Drosophila* cell line samples (reference TEs, INE-1 insertions, and TEs in low recombination regions excluded). Supplementary File S3 includes data matrix of the number of non-reference TE insertion gain events per family on each branch of the most parsimonious tree used for the heatmap in Figure 3B. Supplementary File S4 includes non-redundant bed files from McClintock runs using ngs\_te\_mapper2 module on the normalized OSS and OSC dataset. Supplementary File S5 includes clustered TE profiles in the format of binary presence/absence data matrix including six OSS and OSC cell line samples. Supplementary File S6 includes data matrix of the number of non-reference TE insertion gain events per family on each branch of the most parsimonious tree used for the heatmap in Figure 4C.

## Acknowledgments

The authors thank Nancy Go and Sharon Gorski (Canada's Michael Smith Genome Sciences Centre, BC Cancer) and Michael Strand (University of Georgia) for supplying samples of mbn2 cells; Noah Workman and Magdy Alabady at the University of Georgia Genomics and Bioinformatics Core for assistance with Illumina library preparation and sequencing; Dan Hultmark (Umeå University), Julius Brennecke (Institute of Molecular

Biotechnology, Vienna) and Nelson Lau (Boston University) for information about the history of mbn2, OSS, and OSC cell lines; and Nelson Lau and two anonymous reviewers for helpful comments on the manuscript.

## Funding

This work was supported in part by resources and technical expertise from the Georgia Advanced Computing Resource Center, and by funding from a University of Georgia Research Education Award Traineeship (P.J.B.), the University of Georgia Research Foundation (C.M.B.), and National Institutes of Health grant 2P40OD010949 (A.C.Z.).

## Conflicts of interest

The authors declare that there is no conflict of interest.

## Literature cited

- Adrion JR, Song MJ, Schridder DR, Hahn MW, Schaack S. 2017. Genome-wide estimates of transposable element insertion and deletion rates in *Drosophila melanogaster*. *Genome Biol Evol.* 9: 1329–1340.
- Almeida JL, Cole KD, Plant AL. 2016. Standards for cell line authentication and beyond. *PLoS Biol.* 14:e1002476.
- American Type Culture Collection Standards Development Organization Workgroup ASN-0002. 2010. Cell line misidentification: the beginning of the end. *Nat Rev Cancer.* 10:441–448.
- Babic Z, Capes-Davis A, Martone ME, Bairoch A, Ozyurt IB, et al. 2019. Incidences of problematic cell lines are lower in papers that use RRIDs to identify cell lines. *eLife.* 8:e41676.
- Barallon R, Bauer SR, Butler J, Capes-Davis A, Dirks WG, et al. 2010. Recommendation of short tandem repeat profiling for authenticating human cell lines, stem cells, and tissues. *In Vitro Cell Dev Biol Anim.* 46:727–732.
- Barckmann B, El-Barouk M, Péliousson A, Mugat B, Li B, et al. 2018. The somatic piRNA pathway controls germline transposition over generations. *Nucleic Acids Res.* 46:9524–9536.
- Batzler MA, Deininger PL. 2002. Alu repeats and human genomic diversity. *Nat Rev Genet.* 3:370–379.
- Bergman CM, Quesneville H, Anxolabehere D, Ashburner M. 2006. Recurrent insertion and duplication generate networks of transposable element sequences in the *Drosophila melanogaster* genome. *Genome Biol.* 7:R112.
- Boeva V, Popova T, Bleakley K, Chiche P, Cappo J, et al. 2012. Control-FREEC: a tool for assessing copy number and allelic content using next-generation sequencing data. *Bioinformatics.* 28: 423–425.
- Bray NL, Pimentel H, Melsted P, Pachter L. 2016. Near-optimal probabilistic RNA-seq quantification. *Nat Biotechnol.* 34:525–527.
- Brown JB, Boley N, Eisman R, May GE, Stoiber MH, et al. 2014. Diversity and dynamics of the *Drosophila* transcriptome. *Nature.* 512:393–399.
- Capes-Davis A, Theodosopoulos G, Atkin I, Drexler HG, Kohara A, et al. 2010. Check your cultures! A list of cross-contaminated or misidentified cell lines. *Int J Cancer.* 127:1–8.
- Castro F, Dirks WG, Fähnrich S, Hotz-Wagenblatt A, Pawlita M, et al. 2013. High-throughput SNP-based authentication of human cell lines. *Int J Cancer.* 132:308–314.
- Chakraborty M, VanKuren NW, Zhao R, Zhang X, Kalsow S, et al. 2018. Hidden genetic variation shapes the structure of functional elements in *Drosophila*. *Nat Genet.* 50:20–25.
- Charlesworth B, Langley CH. 1989. The population genetics of *Drosophila* transposable elements. *Annu Rev Genet.* 23:251–287.
- Chen S, Zhou Y, Chen Y, Gu J. 2018. fastp: an ultra-fast all-in-one FASTQ preprocessor. *Bioinformatics.* 34:i884–i890.
- Cherbas L, Willingham A, Zhang D, Yang L, Zou Y, et al. 2011. The transcriptional diversity of 25 *Drosophila* cell lines. *Genome Res.* 21:301–314.
- Cridland JM, Macdonald SJ, Long AD, Thornton KR. 2013. Abundance and distribution of transposable elements in two *Drosophila* QTL mapping resources. *Mol Biol Evol.* 30:2311–2327.
- Currie DA, Milner MJ, Evans CW. 1988. The growth and differentiation in vitro of leg and wing imaginal disc cells from *Drosophila melanogaster*. *Development.* 102:805–814.
- Defendi V, Billingham RE, Silvers WK, Moorhead P. 1960. Immunological and karyological criteria for identification of cell lines. *J Natl Cancer Inst.* 25:359–385.
- Derrien T, Estelle J, Sola SM, Knowles DG, Raineri E, et al. 2012. Fast computation and applications of genome mappability. *PLoS One.* 7:e30377.
- Echalier G. 1997. *Drosophila Cells in Culture*. San Diego, CA: Academic Press.
- Echalier G, Ohanessian A. 1969. Isolement, en cultures in vitro, de lignées cellulaires diploïdes de *Drosophila melanogaster*. *C R Acad Hebd Seances Acad Sci D.* 268:1771–1773.
- Gartler SM. 1967. Genetic markers as tracers in cell culture. *Natl Cancer Inst Monogr.* 26:167–195.
- Gateff E. 1977. New mutants report. *Drosophila Inf Serv.* 52:4–5.
- Gateff E, Gissmann L, Shrestha R, Plus N, Pfister H, et al. 1980. Characterization of two tumorous blood cell lines of *Drosophila melanogaster* and the viruses they contain. (Invertebrate Systems in Vitro Fifth International Conference on Invertebrate Tissue Culture, Rigi-Kaltbad, Switzerland). Amsterdam: Elsevier North-Holland Biomedical Press. p. 517–533.
- Gilbert DA, Reid YA, Gail MH, Pee D, White C, et al. 1990. Application of DNA fingerprints for cell-line individualization. *Am J Hum Genet.* 47:499–514.
- Horbach SPJM, Halfman W. 2017. The ghosts of HeLa: how cell line misidentification contaminates the scientific literature. *PLoS One.* 12:e0186281.
- Huang Y, Liu Y, Zheng C, Shen C. 2017. Investigation of cross-contamination and misidentification of 278 widely used tumor cell lines. *PLoS One.* 12:e0170384.
- Ilyin YV, Chmeliauskaite VG, Ananiev EV, Georgiev GP. 1980. Isolation and characterization of a new family of mobile dispersed genetic elements, m<sub>dg3</sub>, in *Drosophila melanogaster*. *Chromosoma.* 81:27–53.
- Kofler R, Betancourt AJ, Schlotterer C. 2012. Sequencing of pooled DNA samples (pool-seq) uncovers complex dynamics of transposable element insertions in *Drosophila melanogaster*. *PLoS Genet.* 8:e1002487.
- Kofler R, Gomez-Sanchez D, Schlotterer C. 2016. PoPoolationTE2: comparative population genomics of transposable elements using pool-seq. *Mol Biol Evol.* 33:2759–2764.
- Krijthe JH. 2015. Rtsne: T-distributed stochastic neighbor embedding using Barnes-Hut implementation. <https://github.com/jkrijthe/Rtsne>
- Larkin A, Marygold SJ, Antonazzo G, Attrill H, dos Santos G, et al.; FlyBase Consortium. 2021. FlyBase: updates to the *Drosophila melanogaster* knowledge base. *Nucleic Acids Res.* 49:D899–D907.

- Leblanc P, Dastugue B, Vaury C. 1999. The integration machinery of ZAM, a retroelement from *Drosophila melanogaster*, acts as a sequence-specific endonuclease. *J Virol.* 73:7061–7064.
- Lee H, McManus CJ, Cho D-Y, Eaton M, Renda F, et al. 2014. DNA copy number evolution in *Drosophila* cell lines. *Genome Biol.* 15:R70.
- Li H. 2011. A statistical framework for SNP calling, mutation discovery, association mapping and population genetical parameter estimation from sequencing data. *Bioinformatics.* 27:2987–2993.
- Li H. 2015. seqtk. <https://github.com/lh3/seqtk>
- Liang-Chu MMY, Yu M, Haverty PM, Koeman J, Ziegler J, et al. 2015. Human biosample authentication using the high-throughput, cost-effective SNPtrace system. *PLoS One.* 10:e0116218.
- Linheiro RS, Bergman CM. 2012. Whole genome resequencing reveals natural target site preferences of transposable elements in *Drosophila melanogaster*. *PLoS One.* 7:e30008.
- Lorsch JR, Collins FS, Lippincott-Schwartz J. 2014. Fixing problems with cell lines. *Science.* 346:1452–1453.
- Luhur A, Klueg KM, Zelfhof AC. 2019. Generating and working with *Drosophila* cell cultures: Current challenges and opportunities. *Wiley Interdiscip Rev Dev Biol.* 8:e339.
- MacLeod RA, Dirks WG, Matsuo Y, Kaufmann M, Milch H, et al. 1999. Widespread intraspecies cross-contamination of human tumor cell lines arising at source. *Int J Cancer.* 83:555–563.
- Manee MM, Jackson J, Bergman CM. 2018. Conserved noncoding elements influence the transposable element landscape in *Drosophila*. *Genome Biol Evol.* 10:1533–1545.
- Masters JR, Thomson JA, Daly-Burns B, Reid YA, Dirks WG, et al. 2001. Short tandem repeat profiling provides an international reference standard for human cell lines. *Proc Natl Acad Sci U S A.* 98:8012–8017.
- Mohamed M, Dang NT-M, Ogyama Y, Burlet N, Mugat B, et al. 2020. A transposon story: from TE content to TE dynamic invasion of *Drosophila* genomes using the single-molecule sequencing technology from Oxford Nanopore. *Cells.* 9:1776.
- Mohammad TA, Tsai YS, Ameer S, Chen H-IH, Chiu Y-C, et al. 2019. CeL-ID: cell line identification using RNA-seq data. *BMC Genomics.* 20:81.
- Morales V, Straub T, Neumann MF, Mengus G, Akhtar A, et al. 2004. Functional integration of the histone acetyltransferase MOF into the dosage compensation complex. *EMBO J.* 23:2258–2268.
- Nelson MG, Linheiro RS, Bergman CM. 2017. McClintock: an integrated pipeline for detecting transposable element insertions in whole-genome shotgun sequencing data. *G3 (Bethesda).* 7:2749–2762.
- Nelson-Rees WA, Daniels DW, Flandermeyer RR. 1981. Cross-contamination of cells in culture. *Science.* 212:446–452.
- Niki Y, Yamaguchi T, Mahowald AP. 2006. Establishment of stable cell lines of *Drosophila* germ-line stem cells. *Proc Natl Acad Sci U S A.* 103:16325–16330.
- O'Brien SU, Kleiner G, Olson R, Shannon JE. 1977. Enzyme polymorphisms as genetic signatures in human cell cultures. *Science.* 195:1345–1348.
- Osada N, Kohara A, Yamaji T, Hirayama N., Kasai F. et al. 2014. The Genome Landscape of the African Green Monkey Kidney-Derived Vero Cell Line. *DNA Research.* 21:673–683.
- Parson W, Kirchebner R, Mühlmann R, Renner K, Kofler A, et al. 2005. Cancer cell line identification by short tandem repeat profiling: power and limitations. *FASEB J.* 19:434–436.
- Peel DJ, Milner MJ. 1990. The diversity of cell morphology in cloned cell lines derived from *Drosophila* imaginal discs. *Roux Arch Dev Biol.* 198:479–482.
- Potter SS, Brorein WJ, Dunsmuir P, Rubin GM. 1979. Transposition of elements of the 412, copia and 297 dispersed repeated gene families in *Drosophila*. *Cell.* 17:415–427.
- Quinlan AR, Hall IM. 2010. BEDTools: a flexible suite of utilities for comparing genomic features. *Bioinformatics.* 26:841–842.
- Rahman R, Chirn G-W, Kanodia A, Sytnikova YA, Brembs B, et al. 2015. Unique transposon landscapes are pervasive across *Drosophila melanogaster* genomes. *Nucleic Acids Res.* 43:10655–10672.
- Ray DA, Xing J, Salem A-H, Batzer MA. 2006. SINEs of a nearly perfect character. *Syst Biol.* 55:928–935.
- Ress C, Holtmann M, Maas U, Sofsky J, Dorn A. 2000. 20-Hydroxyecdysone-induced differentiation and apoptosis in the *Drosophila* cell line, l(2)mbn. *Tissue Cell.* 32:464–477.
- Rishishwar L, Marino-Ramirez L, Jordan IK. 2017. Benchmarking computational tools for polymorphic transposable element detection. *Brief Bioinformatics.* 18:908–918.
- Robb SMC, Lu L, Valencia E, Burnette JM, Okumoto Y, et al. 2013. The use of RelocaTE and unassembled short reads to produce high-resolution snapshots of transposable element generated diversity in rice. *G3 (Bethesda).* 3:949–957.
- Roy S, Ernst J, Kharchenko PV, Kheradpour P, Negre N, et al.; modENCODE Consortium. 2010. Identification of functional elements and regulatory circuits by *Drosophila* modENCODE. *Science.* 330:1787–1797.
- Saito K, Inagaki S, Mituyama T, Kawamura Y, Ono Y, et al. 2009. A regulatory circuit for piwi by the large Maf gene traffic jam in *Drosophila*. *Nature.* 461:1296–1299.
- Samakovlis C, Asling B, Boman HG, Gateff E, Hultmark D. 1992. In vitro induction of cecropin genes—an immune response in a *Drosophila* blood cell line. *Biochem Biophys Res Commun.* 188:1169–1175.
- Schneider I. 1972. Cell lines derived from late embryonic stages of *Drosophila melanogaster*. *J Embryol Exp Morphol.* 27:353–365.
- Schug MD, Mackay TF, Aquadro CF. 1997. Low mutation rates of microsatellite loci in *Drosophila melanogaster*. *Nat Genet.* 15:99–102.
- Schwartz YB, Kahn TG, Nix DA, Li X-Y, Bourgon R, et al. 2006. Genome-wide analysis of Polycomb targets in *Drosophila melanogaster*. *Nat Genet.* 38:700–705.
- Siensi G, Dönertas D, Brennecke J. 2012. Transcriptional silencing of transposons by Piwi and maelstrom and its impact on chromatin state and gene expression. *Cell.* 151:964–980.
- Singh ND, Petrov DA. 2004. Rapid sequence turnover at an intergenic locus in *Drosophila*. *Mol Biol Evol.* 21:670–680.
- Smukowski Heil C, Patterson K, Shang Hickey AM, Alcantara E, Dunham MJ. 2021. Transposable element mobilization in interspecific yeast hybrids. *Genome Biol Evol.* 13:evab033.
- Sonesson C, Love MI, Robinson MD. 2015. Differential analyses for RNA-seq: transcript-level estimates improve gene-level inferences. *F1000Res.* 4:1521.
- Song S, Nones K, Miller D, Harliwong I, Kassahn KS. et al. 2012. qpure: a tool to estimate tumor cellularity from genome-wide single-nucleotide polymorphism profiles. *PLOS ONE.* 7:e45835
- Stanley CE, Kulathinal RJ. 2016. Genomic signatures of domestication on neurogenetic genes in *Drosophila melanogaster*. *BMC Evol Biol.* 16:6.
- Stoiber M, Celniker S, Cherbas L, Brown B, Cherbas P. 2016. Diverse hormone response networks in 41 independent *Drosophila* cell lines. *G3 (Bethesda).* 6:683–694.
- Sukumaran J, Holder MT. 2010. DendroPy: a Python library for phylogenetic computing. *Bioinformatics.* 26:1569–1571.
- \*Swofford D. 2003. PAUP: Phylogenetic Analysis Using Parsimony (\*and Other Methods). Sunderland, MA: Sinauer Associates.

- Sytnikova YA, Rahman R, Chirn G-W, Clark JP, Lau NC. 2014. Transposable element dynamics and PIWI regulation impacts lncRNA and gene expression diversity in *Drosophila* ovarian cell cultures. *Genome Res.* 24:1977–1990.
- van der Maaten L. 2014. Accelerating t-SNE using tree-based algorithms. *J Mach Learn Res.* 15:3221–3245.
- van der Maaten L, Hinton G. 2008. Visualizing data using t-SNE. *J Mach Learn Res.* 9:2579–2605.
- Vendrell-Mir P, Barteri F, Merenciano M, González J, Casacuberta JM, et al. 2019. A benchmark of transposon insertion detection tools using real data. *Mob DNA.* 10:53.
- Wang J, Keightley PD, Halligan DL. 2007. Effect of divergence time and recombination rate on molecular evolution of *Drosophila* INE-1 transposable elements and other candidates for neutrally evolving sites. *J Mol Evol.* 65:627–639.
- Wen J, Mohammed J, Bortolamiol-Becet D, Tsai H, Robine N, et al. 2014. Diversity of miRNAs, siRNAs, and piRNAs across 25 *Drosophila* cell lines. *Genome Res.* 24:1236–1250.
- Yanagawa S, Lee JS, Ishimoto A. 1998. Identification and characterization of a novel line of *Drosophila* Schneider S2 cells that respond to wingless signaling. *J Biol Chem.* 273:32353–32359.
- Yang N, Srivastav SP, Rahman R, Ma Q, Dayama G, et al. 2021. Transposable element landscape changes are buffered by RNA silencing in aging *Drosophila*. *bioRxiv*. <https://www.biorxiv.org/content/10.1101/2021.01.08.425853v1>
- Yates AD, Achuthan P, Akanni W, Allen J, Allen J, et al. 2020. Ensembl 2020. *Nucleic Acids Res.* 48:D682–D688.
- Yu M, Selvaraj SK, Liang-Chu MMY, Aghajani S, Busse M, et al. 2015. A resource for cell line authentication, annotation and quality control. *Nature.* 520:307–311.
- Yu T, Huang X, Dou S, Tang X, Luo S, et al. 2021. A benchmark and an algorithm for detecting germline transposon insertions and measuring de novo transposon insertion frequencies. *Nucleic Acids Res.* 49:e44.
- Zaaijer S, Gordon A, Speyer D, Piccone R, Groen SC, et al. 2017. Rapid re-identification of human samples using portable DNA sequencing. *eLife.* 6:e27798.
- Zampella JG, Rodić N, Yang WR, Huang CRL, Welch J, et al. 2016. A map of mobile DNA insertions in the NCI-60 human cancer cell panel. *Mob DNA.* 7:20.
- Zanni V, Eymery A, Coiffet M, Zytnicki M, Luyten I, et al. 2013. Distribution, evolution, and diversity of retrotransposons at the flamenco locus reflect the regulatory properties of piRNA clusters. *Proc Natl Acad Sci USA.* 110:19842–19847.
- Zhuang J, Wang J, Theurkauf W, Weng Z. 2014. TEMP: a computational method for analyzing transposable element polymorphism in populations. *Nucleic Acids Res.* 42:6826–6838.

Communicating editor: J. R. Bateman